Journal of Magnetism and Magnetic Materials 424 (2017) 161–173

Contents lists available at ScienceDirect

Journal of Magnetism and Magnetic Materials

journal homepage: www.elsevier.com/locate/jmmm

Analysis of fluid-solid interaction in MHD natural convection in a square cavity equally partitioned by a vertical flexible membrane

S.A.M. Mehryan[a], Mohammad Ghalambaz[a,*], Muneer A. Ismael[b], Ali J. Chamkha[c,d]

[a] Department of Mechanical Engineering, Dezful Branch, Islamic Azad University, Dezful, Iran
[b] Mechanical Engineering Department, Engineering College, University of Basrah, Basrah, Iraq
[c] Mechanical Engineering Department, Prince Mohammad Bin Fahd University, Al-Khobar 31952, Saudi Arabia
[d] Prince Sultan Endowment for Energy and Environment, Prince Mohammad Bin Fahd University, Al-Khobar 31952, Saudi Arabia

ARTICLE INFO

Keywords:
Flexible membrane
Square cavity
Magnetic field
Natural convection
Arbitrary Lagrangian- Eulerian

ABSTRACT

This paper investigates numerically the problem of unsteady natural convection inside a square cavity partitioned by a flexible impermeable membrane. The finite element method with the arbitrary Lagrangian-Eulerian (ALE) technique has been used to model the interaction of the fluid and the membrane. The horizontal walls of the cavity are kept adiabatic while the vertical walls are kept isothermal at different temperatures. A uniform magnetic field is applied onto the cavity with different orientations. The cavity has been provided by two eyelets to compensate volume changes due the movement of the flexible membrane. A parametric study is carried out for the pertinent parameters, which are the Rayleigh number (10^5–10^8), Hartmann number (0–200) and the orientation of the magnetic field (0–180°). The change in the Hartmann number affects the shape of the membrane and the heat transfer in the cavity. The angle of the magnetic field orientation also significantly affects the shape of the membrane and the heat transfer in the cavity.

Greek symbols.

α	thermal diffusivity
β	thermal expansion coefficient
ε	strain
λ	Lame's first constant
μ	dynamic viscosity of fluid
μ_l	Lame's second constant
φ	angle of magnetic field orientation
σ	stress tensor
σ_l	electric conductivity of fluid
τ	dimensionless time
ν	kinematic viscosity
ϕ	electric field
υ	Poisson's ratio
ρ	density
ρ_R	density ratio

Subscripts

avg	average
c	cold
f	fluid
h	hot
P	partition
s	solid

Superscripts

*	dimensional parameters

1. Introduction

The natural convection of fluids in enclosed spaces has been studied extensively due to its vital importance in industrial and engineering

* Corresponding author.
E-mail addresses: a.mansuri1366@gmail.com (S.A.M. Mehryan), m.ghalambaz@iaud.ac.ir (M. Ghalambaz), muneerismael@yahoo.com, muneer.ismael@uobasrah.edu.iq (M.A. Ismael), achamkha@pmu.edu.sa (A.J. Chamkha).

http://dx.doi.org/10.1016/j.jmmm.2016.09.123
Received 30 April 2016; Received in revised form 27 July 2016; Accepted 26 September 2016
Available online 04 October 2016
0304-8853/

Nomenclature

B_o	applied magnetic field
$\mathbf{d}_s$	displacement vector
E	dimensional Young's modulus
E_τ	non-dimensional elasticity modulus
$\mathbf{F}_v$	body force vector
$\mathbf{g}$	gravitational acceleration vector
$\mathbf{Ha}$	Hartmann number vector
Ha	Hartmann number
$\mathbf{J_e}$	electric current density
L	cavity size
P	pressure
Pr	Prandtl number
$\mathbf{Ra}$	thermal Rayleigh vector
Ra	thermal Rayleigh number
t	time
t^*_P	dimensional thickness of the membrane
t_P	dimensionless thickness of the membrane
T	temperature
x,y	Cartesian coordinates
$\mathbf{u}$	velocity vector
$\mathbf{w}$	moving coordinate velocity
W_s	strain energy density function

applications, such as cooling of electronic components, cooling systems in nuclear reactors, solar collector-receivers, insulation and flooding protection for buried pipes used for district heating and cooling, etc. Therefore, interested in natural convection may find a variety of investigations regarding natural convection in enclosures. The effect of enclosure geometry can be concluded from various studies [1–4]. In some applications, the natural convection becomes undesirable phenomenon as in material solidification; hence, the process can be controlled by applying an external magnetic field [5–9]. There are interesting studies about the utilization of magnetic field to control segregations and flow fluctuations in nanofluids [10–13]. Another procedure to control the flow inside cavities is by insertion of baffles or fins [14–18], hence, forming a partly partitioned cavity. The natural convection studies have been developed to handle partitioned cavities composed of two different materials with permeable interface to simulate say the design of building and heat storage systems insulation [19–23].

When the simulation is carried out further by considering impermeable divider to separate two media, the problem can be utilized to model more interesting applications such as a box containing electronic units and divided into partitions using thermal conductive plates. Some of the sensitive electronic equipment should be insulated from the surrounding using a conductive metallic cover. In many cases, a chemical reactor should be divided in sections in which each section contains different chemical species, but the heat transfer could be occurred between the species through partitions. In a solar collector, the convection in the two adjacent air layers couples at the glazing. Hence, the practical application of partitions in enclosures has encouraged researchers to examine the effect of the presence of partitions on convective heat transfer in cavities. Varol et al. [24] considered a diagonally divided square cavity by an inclined plate and filled with a porous medium. They studied the effect of thermal conductivity of the divider plate. Tatsuo et al. [25] wrote a technical note about the limitations of the boundary layer approximation for various positions of a partition. Tatsuo et al. [26] performed an experimental study about natural convection in rectangular enclosure divided by N multiple vertical partitions. They found that the Nusselt number is inversely proportional to the (1+*N*). Oztop et al. [27] studied the natural convection in a differentially heated square enclosure divided by an impermeable partition, where two combinations of air and water were studied on each sub cavity. Kahveci [28] reported a considerable influence of a vertical partition inside an enclosure heated by uniform heat flux. He considered the same fluid filling the two partitions of the enclosure. However, it is essential to consider the transient numerical solution to investigate the transient features of the coupled thermal boundary layers adjacent to a partition that spilt a cavity (Xu et al. [29]), to simulate a time varying thermal boundary conditions (Kalabin et al. [30]), or for the simulation of fluid-structure interaction (Küttler and Wall [31]).

During the last two decades, there is a developing efficient mechanism to enhance the force [32,33] and natural convection heat transfer. One way to enhance the natural convection heat transfer is by exciting the entire cavity or its boundary using an external mechanical force. Hence, this mechanism is unrestricted by the electrical or thermal properties of fluid. The analysis of such problem is classified as moving boundary problem, which encountered in many engineering applications and in nature as well. Cooling fan induced vibration in electronic devices, biological micro-scale experiments, mixing and sterling devices, and heat exchangers are examples of these applications. Fu and Sheih [34,35] simulated the effects of vertical vibration and gravity on the induced convection inside enclosure. Kimoto and Ishidi [36] investigated the vibration effects on the natural convection heat transfer in a square enclosure. Fu et al. [37] reported a remarkable increase in heat transfer associated with laminar forced convection in a parallel-plate channel including an oscillating block. Florio and Harnoy [38] studied the enhancement of natural convection cooling of discrete heat source in a vertical channel using a vibrating plate. Razi et al. [39] reported the convection in porous media undergoing to mechanical vibration. Chung and Vafai [40] investigated the vibrational and buoyancy induced convection in a vertical porous channel with an open-ended top and a vibrating left wall. Cheng et al. [41] proposed a novel approach to enhance the convective heat transfer in heat exchanger by using the flow induced vibration instead of strictly avoiding it.

In some applications, flexible boundaries are oscillating periodically resulting in a deformable domain. For example, flow through diaphragm pump, diaphragm sensors, flow through elastic pipes, as in arteries or other blood vessels, moving pistons or sloshing of fluids in elastic containers [42] and human airways [43,44] are problems of deformable domain. Moreover, this problem is an interested vehicle to mathematicians and those whom delineated in computational fluid dynamics. An efficient numerical simulation technique that deals with this time-dependent moving boundary problem is the arbitrary Lagrangian-Eulerian (ALE) approach [43,44]. It is a developed technique that discourse the drawbacks associated with Lagrangian and Eulerian methods individually. According to ALE technique, the mesh nodes of the computational domain may be moved (according to Lagrangian fashion), held fixed (according to Eulerian fashion), or moved in arbitrary procedure. Details of this technique are illustrated in Hirt et al. [45], Hughes et al. [46], and Donea et al. [47]. Fu and Huang [48] utilized ALE technique to investigate natural convection of a heat plate in vertical channel under vibration motion. One of their main conclusions is that for a given Rayleigh number, natural convection for a certain combination of frequency and amplitude is possibly smaller than that of stationary state.

To the authors' best knowledge, modeling of the hydrodynamic and the heat transfer aspects of the interaction of a flexible structure and a fluid in the presence of a magnetic field has not been addressed yet. This motivates our intent to discover the features of natural convection in a differentially heated cavity containing one or more fluids separated by a thin flexible membrane and subjected to a uniform magnetic field. To make the present study comprehensive, various orientations of the

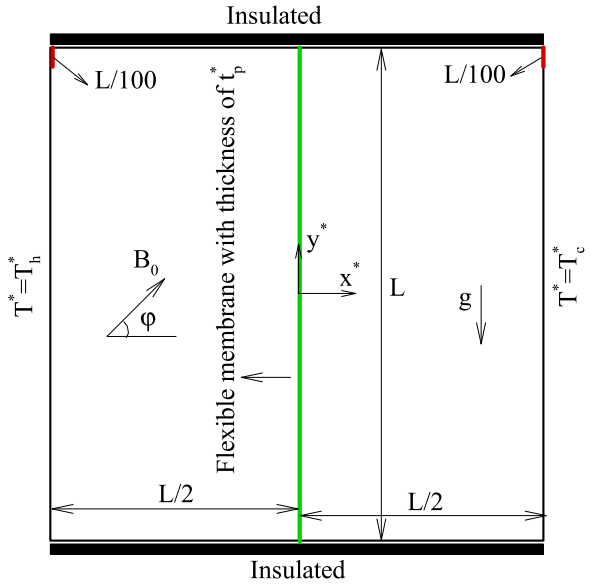

Fig. 1. The schematic view of the problem with the flexible membrane.

magnetic field is considered as well. Moreover, the cavity is provided by two ports to compensate the increase or decrease of fluid volume in both sides due to the membrane deformation. It is sought that the results of this paper are essential in the natural convection heat transfer field.

2. Problem description and mathematical formulation

Fig. 1 shows the schematic representation of the present physical problem and coordinates system employed for driving the governing equations and boundary conditions. Compared with x*, y* dimensions, the z* dimension is assumed very long. So, 2-dimensional mathematical domain is considered. The left and right walls are kept isothermally at T_h^* and T_c^*, respectively, such that $T_h^* > T_c^*$. The bottom and top walls are kept adiabatic. The square cavity has been partitioned into two equal sub-cavities using a vertical thin flexible membrane. The thickness of flexible membrane t_p^* is assumed to be dense, uniform and isotropic. Both sub-cavities have been filled with an incompressible and Newtonian fluid. The flow is unsteady and within the laminar range. The Boussinesq approximation has been employed to describe the fluid density variations in the buoyancy term of the momentum equation. The other properties of the fluid are constant. There is no temperature gradient, heat generation and energy storage in the flexible membrane. This supposition is acceptable when the membrane has very low thickness and high thermal conductivity. Two eyelets have been embedded at the top corners of cavity with the size of L/100, where L is the cavity length. The other walls of the cavity and the membrane are impermeable to mass concentration and have the magnetic permeability of free space. Since the partition is flexible, employing the usual constant pressure points as the pressure constraint is not found to be adequate in the present problem. However, using the open boundary is determined to be possible. The eyelets are selected as small as possible to provide controlled constraints on the pressure distribution in the cavity and not to significantly affect the heat transfer mechanism in the cavity. Further reduction in the size of the cavity can affect the grid quality.

The entire square cavity subjects to the influence of an externally applied, uniform, inclined magnetic field B so that the direction of the magnetic field makes an angle φ with the x*-axis. It is assumed that the interaction between the fluid flow and the external magnetic field has no influence on the magnetic field. In other words, it can be said that the internal induced magnetic fluid and the Joule heating effect are neglected. In addition, the gravity field is acting on the cavity area in the negative y* direction. Viscous dissipation is neglected compared to the convection and diffusion terms. The densities of the fluid and the membrane are equal. In addition, it is assumed that the membrane material is hyper-elastic and reacts nonlinearly against imposed forces.

The effect of the magnetic field on the equations of motion is introduced through the Lorentz force. This force equals to the cross product of the electrical current density $\mathbf{J_e}$ and the magnetic field $\mathbf{B}$ [49]: $\mathbf{F}=\mathbf{J_e}\times\mathbf{B}$. The electric current density $\mathbf{J_e}$ is related to the electric field ϕ and the externally applied magnetic field $\mathbf{B}$ by Ohm's law [49]: , where $\mathbf{u}^*$(u, v) is the fluid velocity vector and σ_l is the electric conductivity of fluid. Since the boundaries of the cavity are electrically insulated, it can be said that the electric field is constant, therefore, (Maxwell's theory). Combining the above two laws results in the following relation [49]: .

Taking into account the above presumptions in writing the governing equations and also with the use of the arbitrary Lagrangian-Eulerian (ALE) technique, the governing equations are as follows:

Continuity equation [23]

$$\nabla^*.\ \mathbf{u}^*=0 \tag{1}$$

Momentums equation [50,51]

$$\frac{\partial \mathbf{u}^*}{\partial t}+(\mathbf{u}^*-\mathbf{w}^*).\ \nabla^*\mathbf{u}^*=-\frac{1}{\rho_f}\nabla^*P^*+\nu_f\nabla^{*2}\mathbf{u}^*+\sigma_l(\mathbf{u}^*\times\mathbf{B})\times\mathbf{B}+\beta\mathbf{g}(T^*-T_c^*) \tag{2}$$

Energy equation [50,51]

$$\frac{\partial T^*}{\partial t}+(\mathbf{u}^*-\mathbf{w}^*).\ \nabla^*T^*=\alpha_f\nabla^{*2}T^* \tag{3}$$

The behavior of the geometrically nonlinear elasto-dynamic structural displacement of the flexible membrane is described by the following nonlinear elasto-dynamic equation [50]:

$$\rho_s\frac{d^2\mathbf{d}_s^*}{dt^2}-\nabla^*\boldsymbol{\sigma}^*=\mathbf{F}_v^* \tag{4}$$

In Eqs. (1)–(4), u^* and v^* are the components of $\mathbf{u}^*$ in x* and y* directions, respectively, $\mathbf{w}^*$ refers to the moving coordinate system velocity vector, $\mathbf{w}^*=(u_s^*,v_s^*)$, u_s and v_s^* are the components of $\mathbf{w}^*$ in x* and y* directions, respectively. P^* is the fluid pressure, T^* is the fluid temperature, $\mathbf{g}$ is the gravity acceleration vector. ∇^* represents the dimensional gradient operation, $\mathbf{d}_s^*$ is the displacement vector of membrane such that $d\mathbf{d}_s^*/dt=\mathbf{w}^*$, $\boldsymbol{\sigma}^*$ is the solid stress tensor, $\mathbf{F}_v^*$ denotes the body forces applied to the flexible membrane. This force can be caused by the gravitational or magnetic fields. Due to the assumptions made, this force is zero. α_f and ν_f are thermal diffusivity and kinematic viscosity of the fluid, respectively, and β is volumetric thermal expansion coefficient. The imposed boundary conditions are:

$$\begin{aligned}&\text{On all walls of the cavity } u^*=v^*=0\\&\text{On the top and bottom walls of the cavity } \frac{\partial T^*}{\partial y^*}=0\\&\text{On the left side wall of the cavity } T^*=T_h^*\\&\text{On the right side wall of the cavity } T^*=T_c^*\end{aligned} \tag{5}$$

Neo-Hookean solid model has been employed to define the stress tensor in Eq. (4). This model is valid when the material of membrane is hyper-elastic and can be applied for showing the nonlinear stress-strain trend of materials with large deformations [50]:

$$\boldsymbol{\sigma}^*=J^{-1}FSF^T \tag{6}$$

where

$$F=(I+\nabla^*\mathbf{d}_s^*),\ \ J=\det(F)\ \text{and}\ S=\partial W_s/\partial\varepsilon \tag{7}$$

The superscript T denotes the transpose of matrix F. W_s and ε are

the strain energy density function and the strain, respectively, they are given by:

$$W_s=\frac{1}{2}\mu_l(J^{-}I_1-3)-\mu_l\ln(J)+\frac{1}{2}\lambda(\ln(J))^2 \tag{8}$$

$$\varepsilon=\frac{1}{2}(\nabla^*\mathbf{d}_s^*+\nabla^*\mathbf{d}_s^{*T}+\nabla^*\mathbf{d}_s^{*T}\nabla^*\mathbf{d}_s^*) \tag{9}$$

where

$$\lambda=\frac{E\nu}{(1+\nu)(1-2\nu)},\ \mu_l=\frac{E}{2(1+\nu)}$$

are Lame's first and second constants, respectively. E and ν are the Young's modulus and the Poisson's ratio, respectively. I_1 refers to the first invariant of the right Cauchy-Green deformation tensor. The simulation of fluid-solid interaction (FSI) has been done using the continuity of kinematic forces and dynamic motions at the membrane surfaces. The mathematical relationships for these two conditions are as follows:

$$\frac{\partial\mathbf{d}_s^*}{\partial t}=\mathbf{u}^* \text{ and } \boldsymbol{\sigma}^*.\ n=-P^*+\mu_f\nabla^*\mathbf{u}^* \tag{10}$$

By writing the energy equation for the membrane with the assumption of no energy generation and storage at the membrane, we obtain

$$\frac{\partial T^{*+}}{\partial n}=\frac{\partial T^{*-}}{\partial n}\ and\ T^{*+}=T^{*-} \tag{11}$$

Positive and negative superscripts refer to the right and left walls of the membrane, respectively. For both eyelets embedded on the vertical side walls, the following boundary condition is always established:

$$[-P^*+\mu_f\nabla^*\mathbf{u}^*].\ n=0 \tag{12}$$

In this equation, n is the unit vector perpendicular to the flexible membrane. Here, in order to make the problem non-dimensional, the following dimensionless parameters are introduced:

$$\mathbf{d}_s=\frac{\mathbf{d}_s^*}{L},\ \boldsymbol{\sigma}=\frac{\boldsymbol{\sigma}^*}{E},\ \tau=\frac{t\alpha_f}{L^2},\ (x,y)=\frac{(x^*,y^*)}{L},\ t_p=\frac{t_p^*}{L},\ \mathbf{u}=\frac{\mathbf{u}^*L}{\alpha_f} \tag{13a}$$

$$\mathbf{w}=\frac{\mathbf{w}^*L}{\alpha_f},\ P=\frac{L^2}{\rho_f\alpha_f^2}P^*,\ T=\frac{T^*-T_c^*}{T_h^*-T_c^*},\ \nabla^*=\frac{\nabla}{1/L},\ \nabla^{*2}=\frac{\nabla^2}{1/L^2} \tag{13b}$$

$$\mathrm{Pr}=\frac{\nu_f}{\alpha_f},\ \mathbf{F}_v=\frac{(\rho_f-\rho_s)L\mathbf{g}}{E},$$
$$E_\tau=\frac{EL^2}{\rho_f\alpha_f^2},\ Ra=\frac{g\beta(T_h^*-T_c^*)L^3}{\nu_f\alpha_f} \tag{13c}$$

$$\rho_R=\frac{\rho_f}{\rho_s},\ \mathbf{Ha}=L\mathbf{B}\sqrt{\frac{\sigma}{\mu}} \tag{13d}$$

Substituting the parameters (13a) and (13b) in the governing equations and using the parameters (13c) and (13d) results in the following dimensionless equations:

$$\frac{1}{\rho_R}\frac{d^2\mathbf{d}_s}{d\tau^2}-E_\tau\nabla\boldsymbol{\sigma}=E_\tau\mathrm{F}_v \tag{14}$$

$$\nabla.\ \mathbf{u}=0 \tag{15}$$

$$\frac{\partial\mathbf{u}}{\partial\tau}+(\mathbf{u}-\mathbf{w}).\ \nabla\mathbf{u}=-\nabla P+\mathrm{Pr}\nabla^2\mathbf{u}+\mathrm{PrRa}T+\mathrm{Pr}(\mathbf{u}\times\mathbf{Ha})\times\mathbf{Ha} \tag{16}$$

$$\frac{\partial T}{\partial\tau}+(\mathbf{u}-\mathbf{w}).\ \nabla T=\nabla^2T \tag{17}$$

In Eqs. (14)–(17), Pr, E_τ, F_v, Ha, ρ_R and **Ha** are the Prandtl number, non-dimensional elasticity modulus, non-dimensionless body force vector, Rayleigh number, the density ratio number and the Hartmann number vector, respectively. It should be noted that **Ha** has two components; Ha sin(φ) and *Ha* cos(φ) along x and y-axes, respectively. The body force term due to the magnetic field can be rewritten in the Cartesian coordinates as $\mathrm{Pr}\,\mathrm{H}_a^2(V\sin\varphi\cos\varphi-u\sin^2\varphi)$ in the x-direction and $\mathrm{Pr}\,\mathrm{H}_a^2(u\sin\varphi\cos\varphi-u\cos^2\varphi)$ in the y-direction. As mentioned, it is assumed that $\rho_s=\rho_f$, therefore it is obvious that the body force imposed to the membrane Fv is zero. This condition is adopted at all stages of solution. Here, it should be noted that the non-dimensional value of the thickness defined for the membrane is 0.012.

The boundary conditions can be rewritten in dimensionless form as follows:

On all walls of the cavity $u=v=0$

On the top and bottom walls of the cavity $\frac{\partial T}{\partial y}=0$

On the left wall of the cavity $T=1$

On the right wall of the cavity $T=0$

For the flexible membrane $\frac{\partial T^+}{\partial n}=\frac{\partial T^-}{\partial n}$ and $T^+=T^-$ (18)

On the fluid-solid interface:

$$\frac{\partial\mathbf{d}_s}{\partial\tau}=\mathbf{u} \text{ and } E_\tau\boldsymbol{\sigma}.\ n=-P+\mathrm{Pr}\nabla\mathbf{u} \tag{19}$$

At both eyelets:

$$[-P+\mathrm{Pr}\nabla\mathbf{u}].\ n=0 \tag{20}$$

At t=0, the fluid is motionless inside the whole cavity domain. Hence, in this situation $u(x,y,0)=0$. The initial temperature in the left and right sub-cavities is T_h and T_c, respectively.

The Nusselt number is representative of the heat transfer rate in the cavity. The convective heat transfer at the left wall can be written as: $q''=h(T_h^*-T_c^*)$ and the conduction heat transfer at the wall can be written as $q''=-k\frac{\partial T^*}{\partial x^*}\big|_{x^*=0}$. Based on the energy balance at a surface, the conduction heat transfer at the surface equals to the convective heat transfer which yields $h_y(T_h^*-T_c^*)=-k\frac{(T_h^*-T_c^*)}{L}\frac{\partial T}{\partial x}\big|_{x=0}$ and finally, the local Nusselt number is obtained as:

$$Nu_{local}=\frac{h_yL}{k}=-\frac{\partial T}{\partial x}\bigg|_{x=0} \tag{21}$$

The average Nusselt number Nuavg is achieved by integrating the local Nusselt number Nulocal:

$$Nu_{avg}=-\int_0^1 Nu_{local}\,dy \tag{22}$$

Another parameter of importance examined in this study is the average temperature inside whole cavity that the following relation calculates it:

$$T_{avg}=\frac{\int T_{local}\,dA}{\int dA} \tag{23}$$

The stream function ψ is defined to describe the fluid motion and can be expressed as follows:

$$u=\frac{\partial\psi}{\partial y},\ v=-\frac{\partial\psi}{\partial x} \tag{24}$$

3. Numerical approach and validation

Because the equations (13)–(16) along with their boundary conditions are non-linear and interdependent, it is necessary that an iterative numerical method be employed to solve them. Therefore, these equations are transformed into the weak form and numerically solved based on the Galerkin finite element method. The details of this

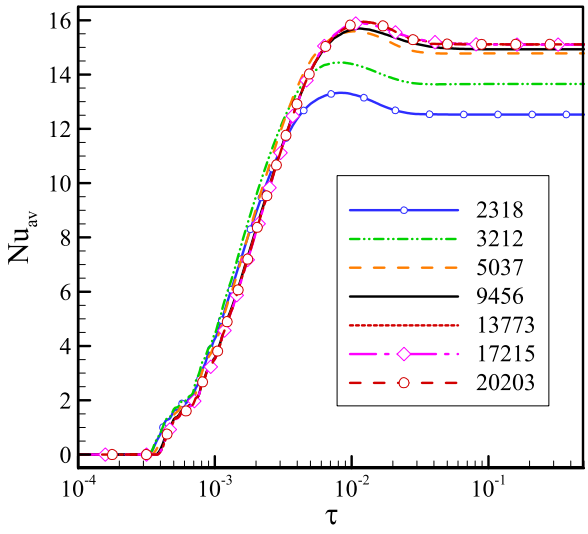

Fig. 2. Variations of average Nusselt number on the hot wall according to the dimensionless time for different grid size at $Ra=10^8$, $Ha=0$, $E_\tau=10^{14}$.

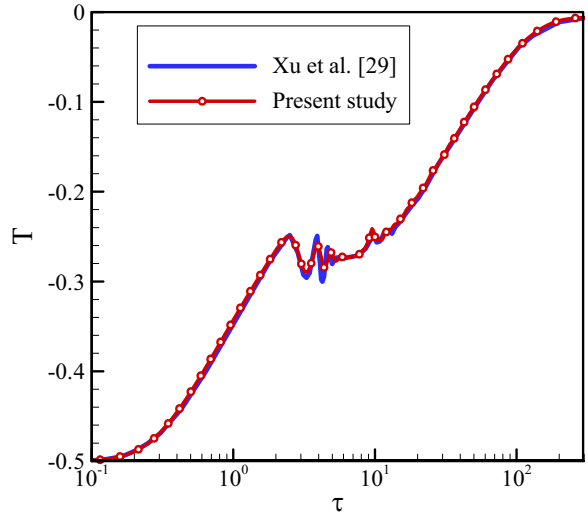

Fig. 3. Comparison with Xu et al. [29] in the case of square cavity divided into two parts by a rigid membrane.

procedure are entirely described in [52]. The computational domain is meshed by applying non-uniform triangular grids. The calculations are terminated in any time step that the error is less than 10^{-7}. An automatic time step procedure is employed to monitor the solution time step accuracy and numerical convergence.

3.1. Grid independency test

To ensure that the obtained results are independent of the number of mesh elements, a grid independency test is achieved. For this purpose, the variations of the Nusselt number according to dimensionless time are investigated on the hot wall for different grids at $Ra=10^8$, $Ha=0$ and $\varphi=0$. Fig. 2 shows the result of this assessment. Because the variations of the average Nusselt number versus time are not significant for the grid size more than 13,773, this grid size has been used to represent of the results.

3.2. Validation

To validate the method used, our results have been compared with the results reported in several published literatures. In the first validation, we have evaluated the correctness and accuracy of our

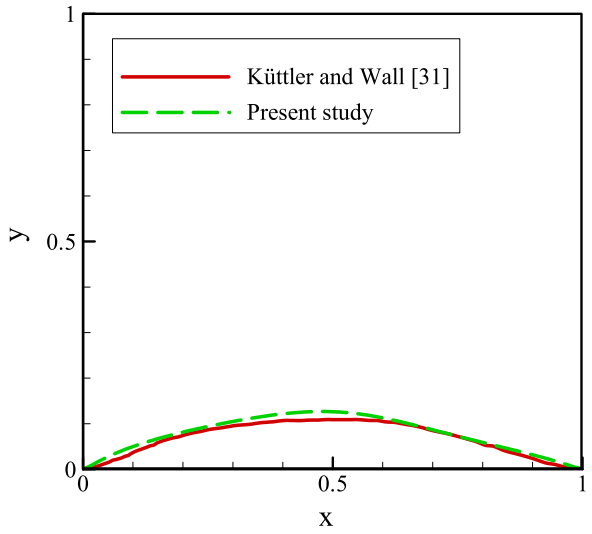

Fig. 4. The deformation of the flexible bottom wall of the lid-driven cavity perused by Küttler and Wall [31], and the present study at t=7.5 s in a dimensional case with the led velocity of u_x=(1-cos(2πt/5)) m/s, ν_f=0.01 m^2/s, ρ_f=1 kg/m^3, E=250 N/m^2, ρ_s=500 kg/m^3 and t^*_p=0.002 m.

results with those obtained by Xu et al. [29] as depicted in Fig. 3. This validation includes comparing the dimensionless temperature reported by [29] and the temperature in the current study at the specified point (0.0083, 0.375). It is necessary to mention that the definition of the dimensionless time in our investigation and Xu et al. [29] is different. The dimensionless time defined by Xu et al. is $\tau=t\alpha Ra^{1/2}/L^2$.

In another validation (Fig. 4), the deformation curve of the bottom wall of a lid-driven square cavity have been compared in our study and the investigation performed by Küttler and Wall [31]. Here, also the accuracy of the solution has been confirmed.

Considering the magnetic effects and for a regular cavity without a partition, the results of the present study can be compared with the results of the study of Sathiyamoorthy and Chamkha [7]. Sathiyamoorthy and Chamkha [7] have studied the natural convective heat transfer in the presence of a magnetic field. Fig. 5 illustrates a comparison between the streamlines and isotherms patterns obtained in the present study and those reported by [7]. This figure shows that the results of the present study are in good agreement with those available in the literature.

One of the most important validations is comparing the experimental results represented by Tatsuo et al. [26] and the numerical results obtained by the present numerical code. The experimental study of [26] includes an examination of the natural convection heat transfer and flow in a rectangular cavity (the ratio of height to length or AR=4) divided into several sub-cavities using the rigid thin surfaces. The thermal conditions imposed on the boundaries of their cavity and the cavity in present study is the same. Fig. 6 compares the results of the current simulation with experimental consequences of Tatsuo et al. and Churchill's relation [53]. In the figure, N shows the number of the rigid plates dividing cavity. It is evident that our numerical simulation accuracy is very good.

4. Results and discussion

The results of this investigation have been presented in this section. In the present study, the influence of controlling parameters such as Rayleigh number ($10^5 \le Ra \le 10^8$), Hartmann number ($0 \le Ha \le 200$) and inclination angle of magnetic field ($0 \le \varphi \le 180°$) on the streamlines and isotherms patterns, the heat transfer rate and the average temperature inside the entire cavity are investigated. While the parameters ρ_R and E_τ are kept fixed at 1 and 10^{14}, respectively. Water is selected as the working fluid with Pr=6.2.

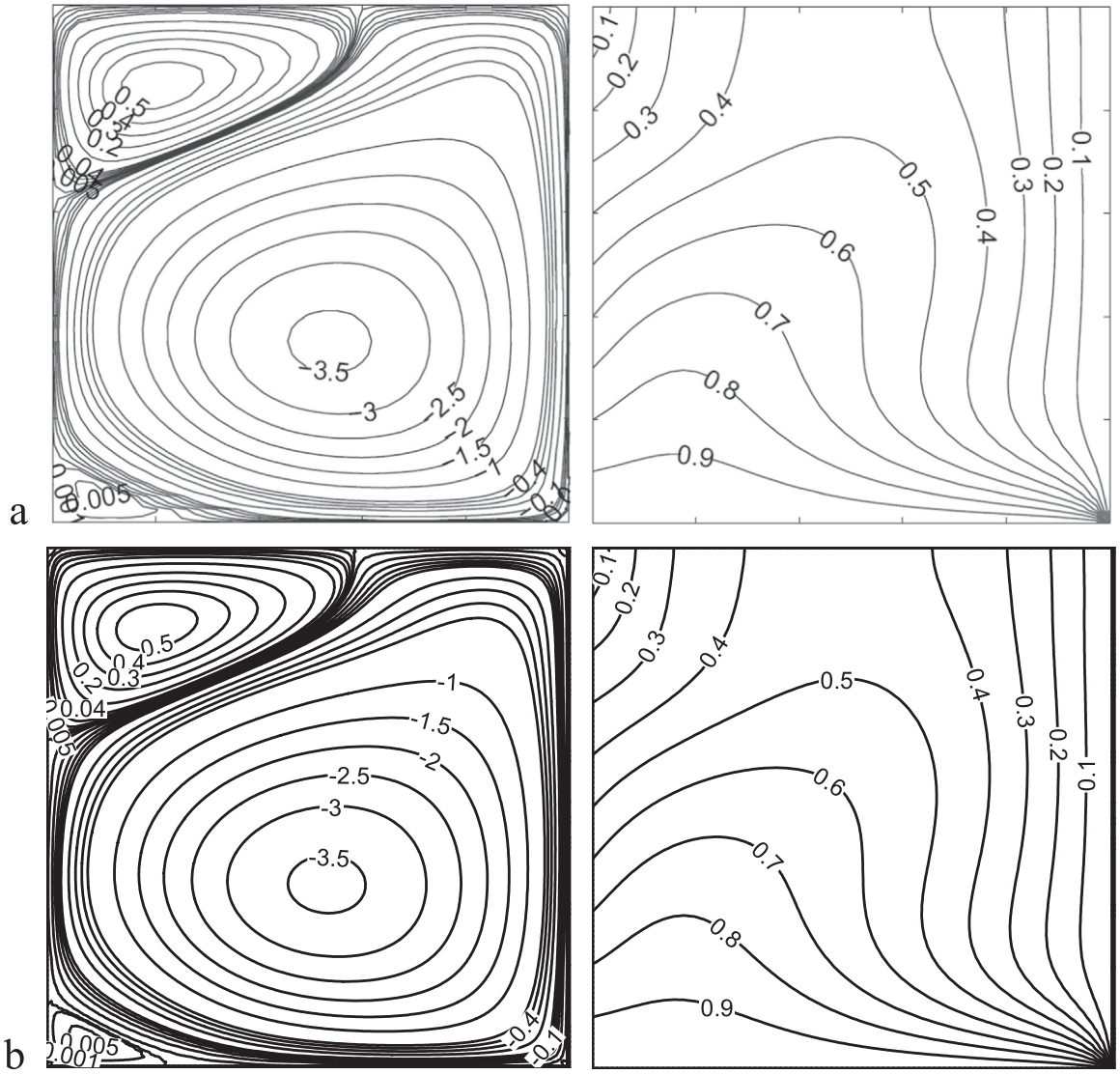

Fig. 5. Comparison of the streamlines and isotherms patterns reported by Sathiyamoorthy and Chamkha [7] (a) and the results of the present study (b) for Ra=10^5, Ha=50, φ=0, Pr=0.025 for a cavity without a partition.

Fig. 7 displays the steady-state streamlines contours for different values of Ha and Ra at φ=2π/3. At the lower range of the studied value of Ra (Ra=10^5), a central weak vortex is formed inside each sub-cavity. Increasing Ra means increasing the buoyancy force in the momentum equation; hence, it is obvious that for all Ha, the strength of vortices formed in both sub-cavities $|\psi|_{max}$ increases when Ra increases. It can be seen that the vortices formed in both sub-cavities are extended horizontally as Ra increases. In some cases, this extension continues until each vortex breaks up into two vortices. On the other hand, the strength of the fluid flow decreases as Ha increases. In fact, the magnetic field plays the role of a drag force that acts at odds with the buoyancy force. The chance that the vortices split into two vortices is reduced as the magnetic field strength or Ha increases. It is interesting to note that at Ha=200 and Rayleigh numbers of Ra=10^5 and Ra=10^6, the vortices extend diagonally with respect to each sub-cavity. However, when the heated fluid hits the top horizontal wall, it falls with the aid of gravity forming clockwise vortices. The right sub-cavity vortex is stronger than that of the left, so the flexible membrane stretched to the left. Furthermore, it is interesting to note that although an increment in the Hartmann number reduces the strength of the fluid flow, it has no effect on the steady state condition of the flexible membrane.

The effects of Ra and Ha on the temperature distribution at φ=2π/3 are shown in Fig. 8. The isotherms patterns shown in Fig. 8 represent how the predominant mechanism heat transfer changes with the variation of Ra and Ha. As seen, the lines of isotherms contours tend to stratify horizontally as Ra increases. This result can be attributed to the increase of the strength of the fluid flow due to an increase in the buoyancy effect. In addition; Fig. 8 shows that for Ra=10^5–10^6 the isotherms look mostly parallel to the vertical walls more and more with the increase of Ha owing to the predomination of conduction mechanism of heat transfer against advection mode.

Figs. 9 and 10 illustrate the influence of the Rayleigh number Ra and the Hartmann number Ha on the average Nusselt number and the mean temperature inside whole cavity according to the dimensionless time. As observed, at the initial stages of natural convection, the average Nusselt number at the hot wall is exactly zero for all Ra and Ha values. This result is perfectly acceptable because initially, the fluid has no any external driving force and the natural convection flow not induces yet. With time evolution, the fluid thermal mixing increases, the heat transfer rate also increases by the advection mechanism. Also, it is found that the average Nusselt number overshoots before reaching steady state at the high values of Ra (Ra=10^7–10^8). The variations of the dimensionless temperature versus time represent that the average temperature inside whole cavity is exactly 0.5 for the initial stages. This result coincides with the defined initial conditions. Afterwards, the

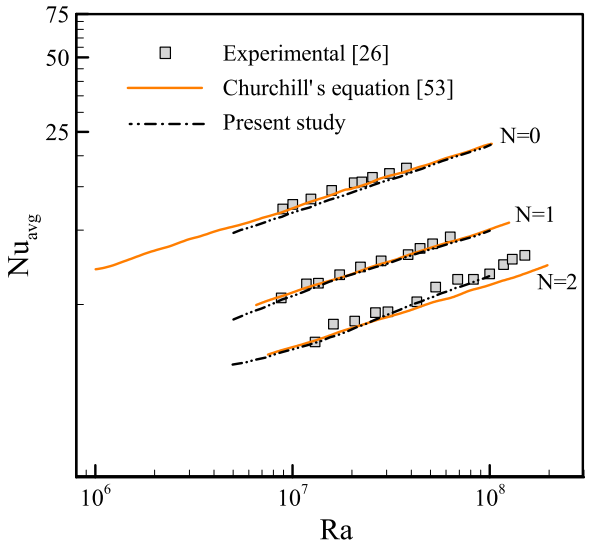

Fig. 6. Comparison between the average Nusselt number obtained in the present study and the experimental data represented by Nishimura et al. [26] and the Churchill's relation [46] for a rectangular enclosure with various rigid partitions (*N*) versus Rayleigh number when *AR*=4 and *Pr*=6.

temprature decreases until it reaches its minimum value, finally, the average temperature rises up until reaching a constant value at the steady state condition. These graphs also indicate that the minimum values of the average temperature with time decreases with increasing *Ha* and *Ra*.

At the beginning, the left sub-cavity connected to the hot wall is at a uniform temperature T^*_h (i.e. T=1) while the right sub-cavity connected to the cold temperature is at a uniform temperature T^*_c (i.e. T=0). The volumes of both sub-cavities are equal, and hence, the average temperature in the cavity is exactly T_{avg}=0.5 at the very early stage of heat transfer. As both sides of the membrane are at different non-dimensional temperatures of 0 and 1, the heat transfer between the sub-cavities commences. The heat transfer in the vicinity of the membrane influences the temperature distribution in the cavity, and as a result, the average temperature of the fluid in the cavity changes. It should be noted that at the very early stages of heat transfer, the temperature of the fluid next to the vertical walls is equal to the temperature of the wall (because of the initial conditions), and hence, the average Nusselt number is zero. Indeed, the temperature in the cavity in the vicinity of the membrane starts to change, and consequently, it affects the average temperature. However, the heat flux next to the vertical walls is zero because of the lack of temperature gradient in the vicinity of the hot or cold walls. After elapsing a sufficient time, the temperature gradient from the area in the vicinity of the membrane develops into the inner regions of the sub-cavities and into the vertical

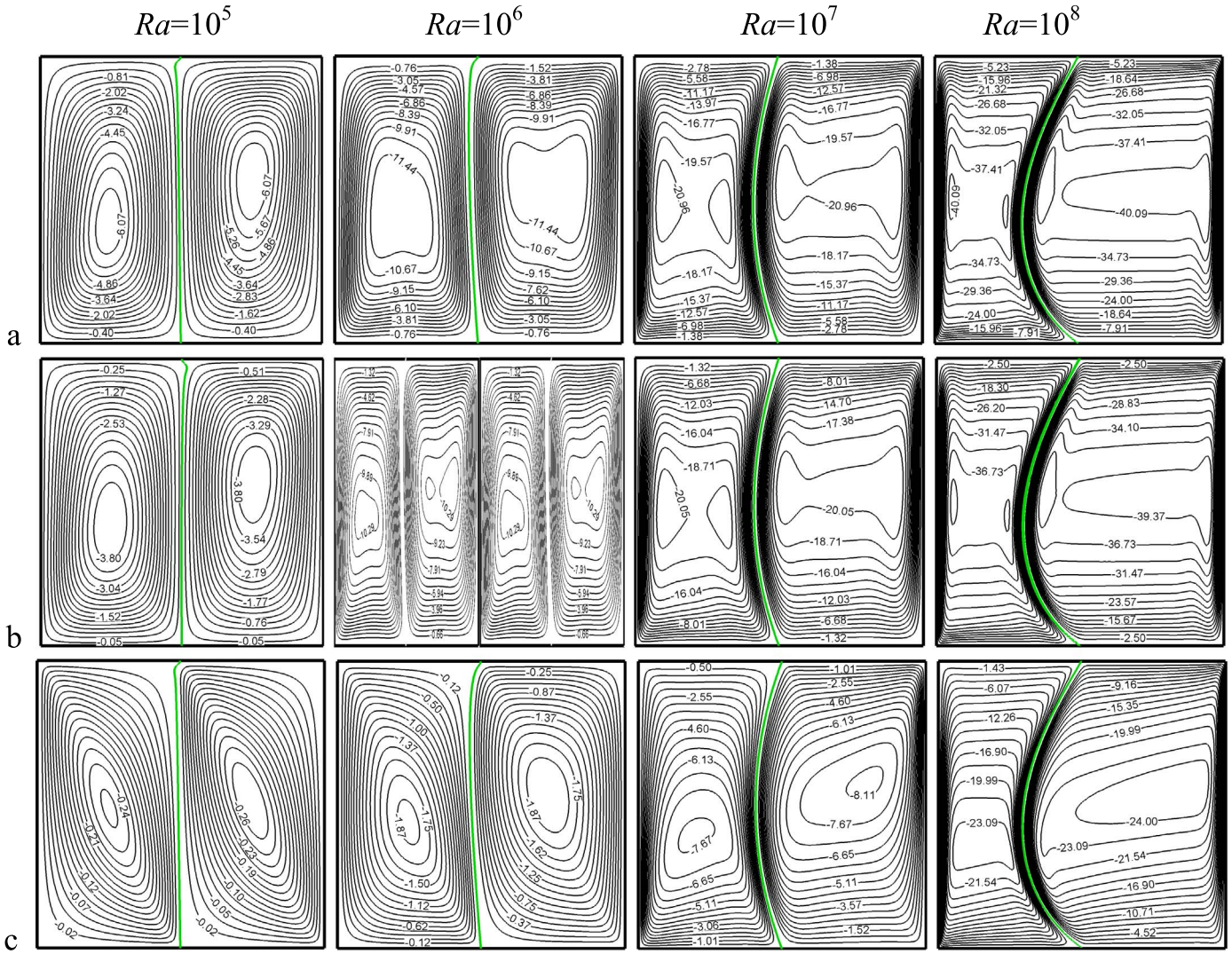

Fig. 7. Streamlines contours for the different values of *Ra* and a: *Ha*=0, *b: Ha*=25 and *Ha*=200 at $\varphi=2\pi/3$.

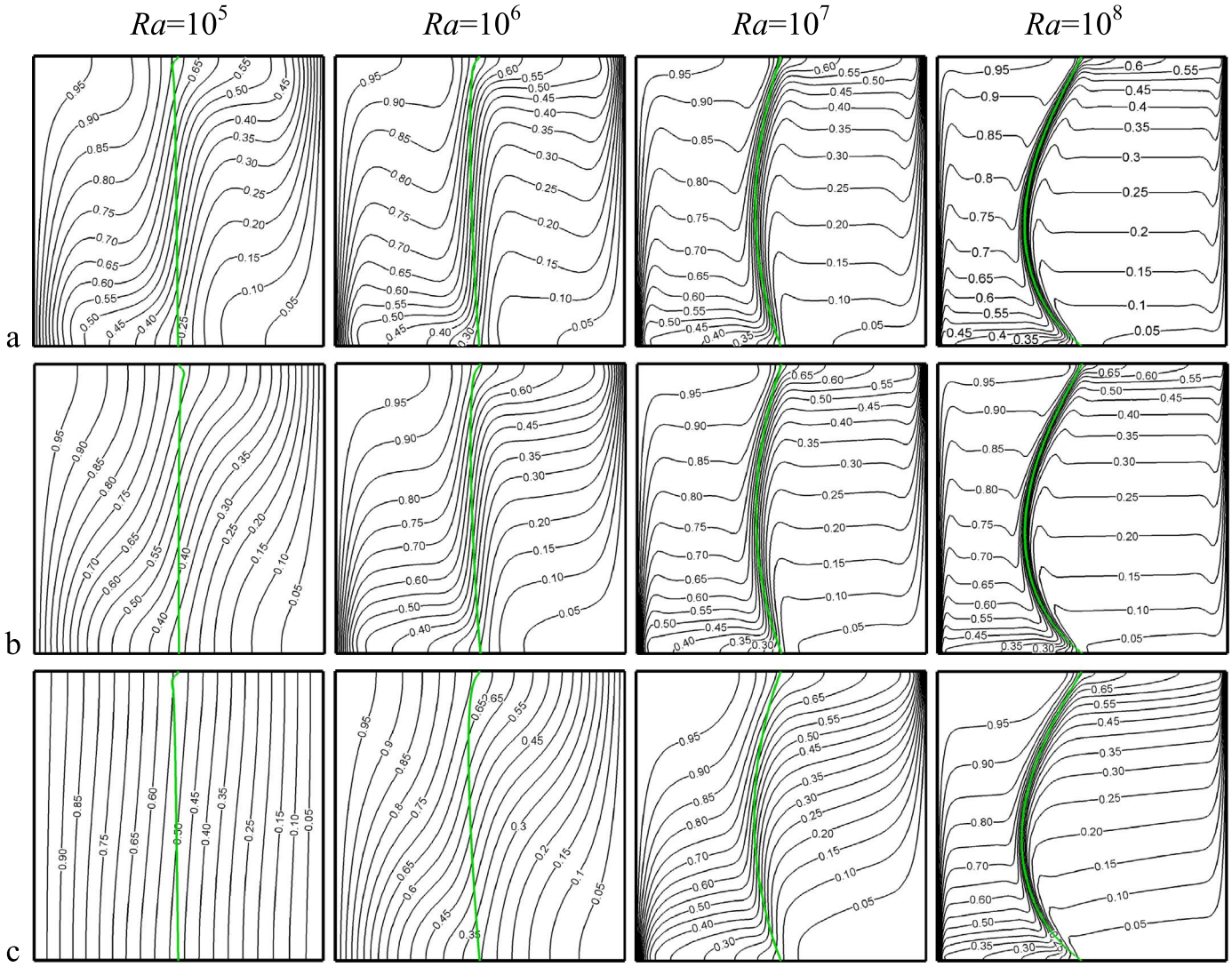

Fig. 8. Isotherms contours for the different values of *Ra* and a: *Ha*=0, *b: Ha*=50 and *Ha*=200 at $\varphi=2\pi/3$.

walls by advective and diffusive heat transfer mechanisms. As the temperature of the fluid finally changes next to the vertical walls, the heat transfer from the wall commences, and the average Nusselt number at the wall starts to raise from zero. For relatively small values of Rayleigh numbers ($Ra=10^5$, 10^6), the time required for a temperature gradient to develop in the cavity from the membrane to a vertical

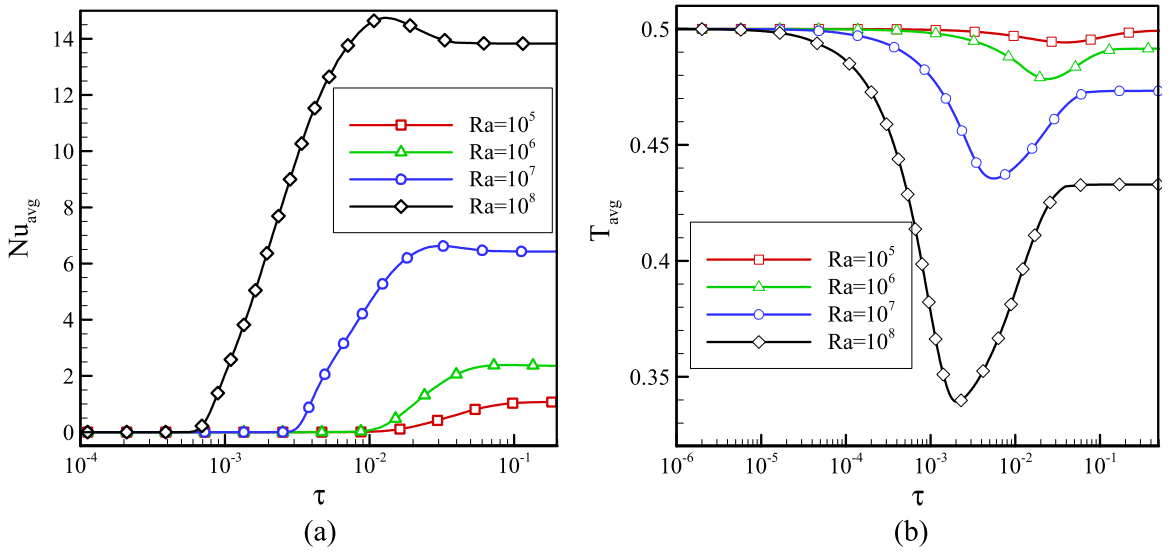

Fig. 9. The variations of average Nusselt number on the hot wall and dimensionless temprature versus the dimentionless time for the different values of *Ra* at *Ha*=100, $\varphi=2\pi/3$.

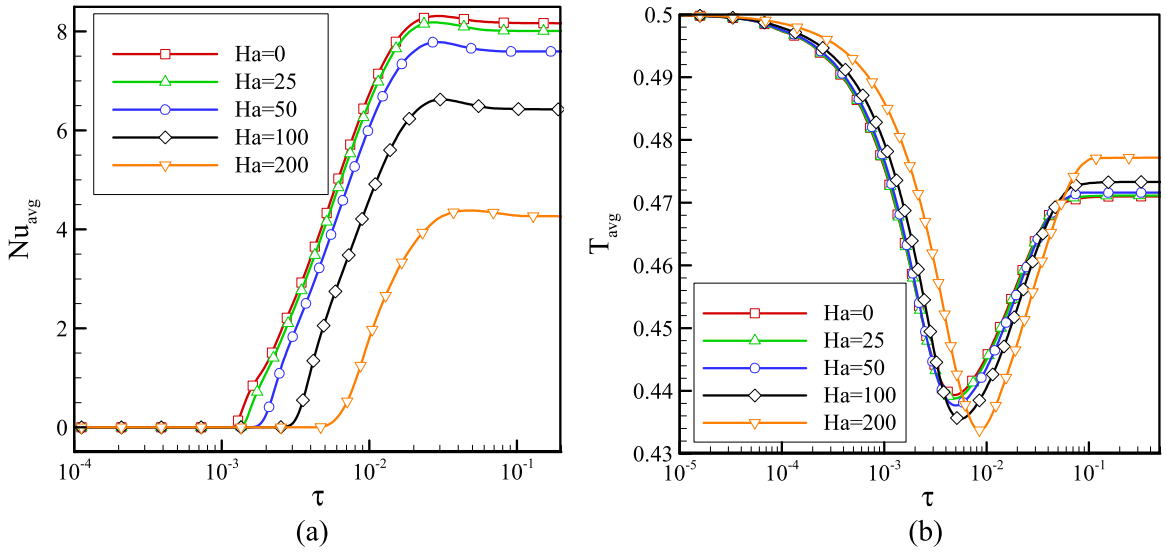

Fig. 10. The variations of average Nusselt number on the hot wall and dimensionless temprature versus the dimentionless time for the different values of *Ha* at $Ra=10^7$, $\varphi=2\pi/3$.

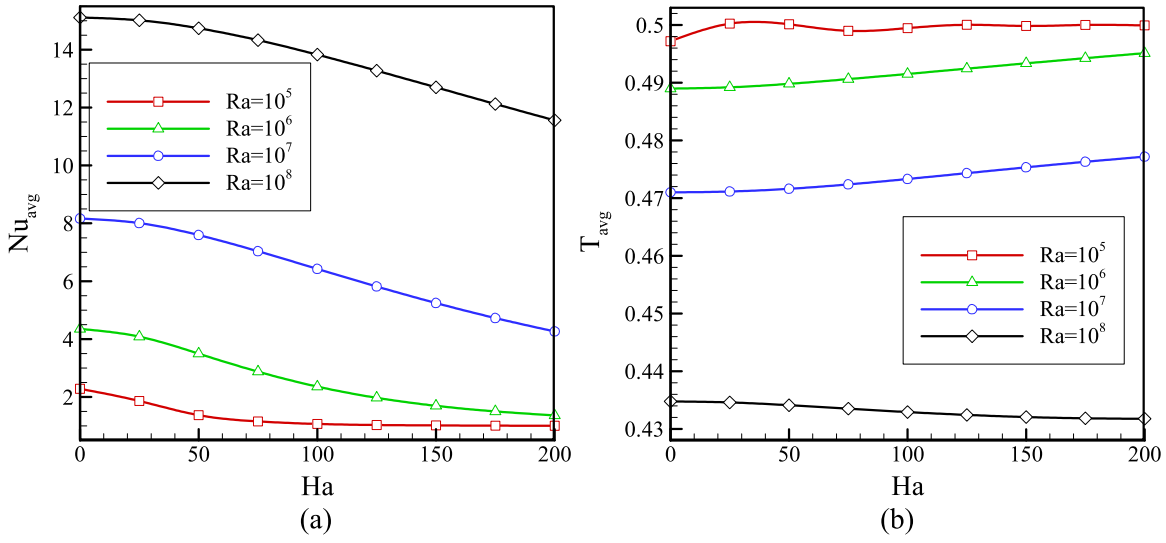

Fig. 11. Average Nusselt number on the hot wall and dimensionless temprature as function of Hartmann number for the different values of *Ra* at $\varphi=2\pi/3$. *Ha*=50 *Ha*=200.

wall is about 10^{-2}. It is clear that as the Rayleigh number increases, the heat transfer mechanism gets stronger, and hence, the time scale required for developing a temperature gradient from the membrane to the wall drops to $\tau=10^{-3}$ in the case of $Ra=10^8$.

As mentioned in the description of Figs. 9 and 10, at the very early stages of heat transfer, when the non-dimensional time is very small (i.e. $\tau\approx10^{-3}$), the heat transfer commences next to the membrane. As the fluid is initially quiescent, the heat transfer next to the membrane takes place moslty by diffusion. Hence, it should be noted that the variation of the inclination angle or the Hartmann number only affects the fluid through the momentum equations (i.e. they only affect the motion of the fluid) when τ is small. Therefore, as seen in Fig. 14(b), the variations of the average temperature for various inclination angles is the same as they have no significant influence on the conduction (diffusive) heat transfer mechanism. The reason for the observed decrease of the average temperature in the cavity is the decreasing trend of the volume of the hot sub-cavity due to the movement of the membrane into the left side (as depicted in Figs. 8 or 12 in the steady-state situation). Therefore, as the membrane moves toward the hot wall, the volume of the hot cavity reduces and volume of the cold cavity increases, and hence, the average temperature, which is defined as the average temperature over all of the cavity decreases. After a while, the advective mechanism of heat transfer in the cavity gets stronger and tends to change the temperature profiles toward the steady state situation. At this stage (τ higher than 10^{-2}), the volume of the hot cavity is smaller, or it can be said that the membrane is closer to the hot wall compared with its distance to the cold wall (see Figs. 8 or 12 which depict the steady state shape of the membrane). As the hot wall is closer to the membrane, the range of the temperature distribution in the hot cavity is closer to the temperature of the hot wall ($T=1$) compared to the case of the cold cavity which is a wider sub-cavity. Therefore, it can be concluded that as the convective heat transfer gets stronger (τ higher than 10^{-2}), the average temperature of the cavity smoothly rises to a constant steady average temperature. The average temperature at the steady state is lower than the initial mean temperature of the 0.5 due to the shape of the membrane and the final smaller size of the hot cavity. For the time snaps of τ higher than 10^{-2}, the effect of variation of the inclination angle is obvious.

The average Nusselt number exhibits almost a monotone trend of behavior. As mentioned, at the very early stage of heat transfer (i.e. $\tau\approx10^{-3}$), the average Nusselt number is zero because of the lack of temperature gradient at the hot wall. After a while, the advective heat transfer mechanisms gets stronger, and a flow of a cold fluid, coming from the membrane, reaches the hot wall. Therefore, as the convective

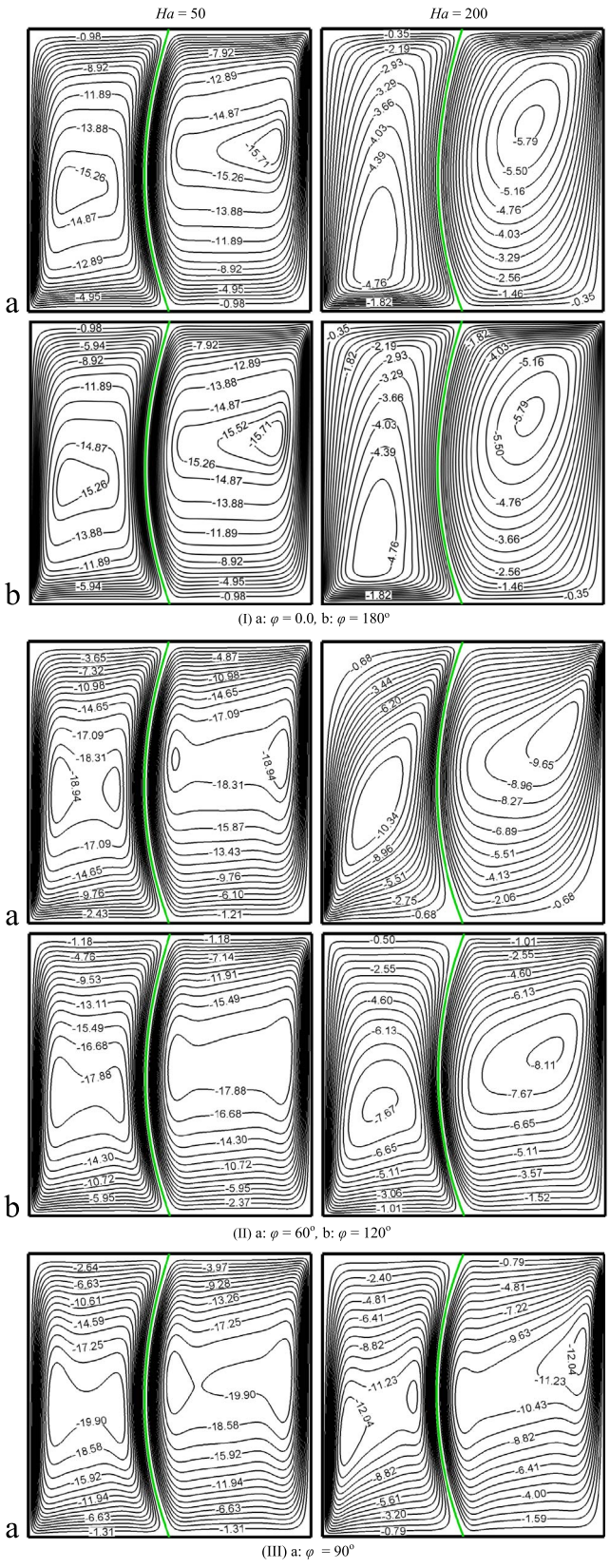

Fig. 12. Streamlines contours for Ha=50 and Ha=200 when Ra=10^7.

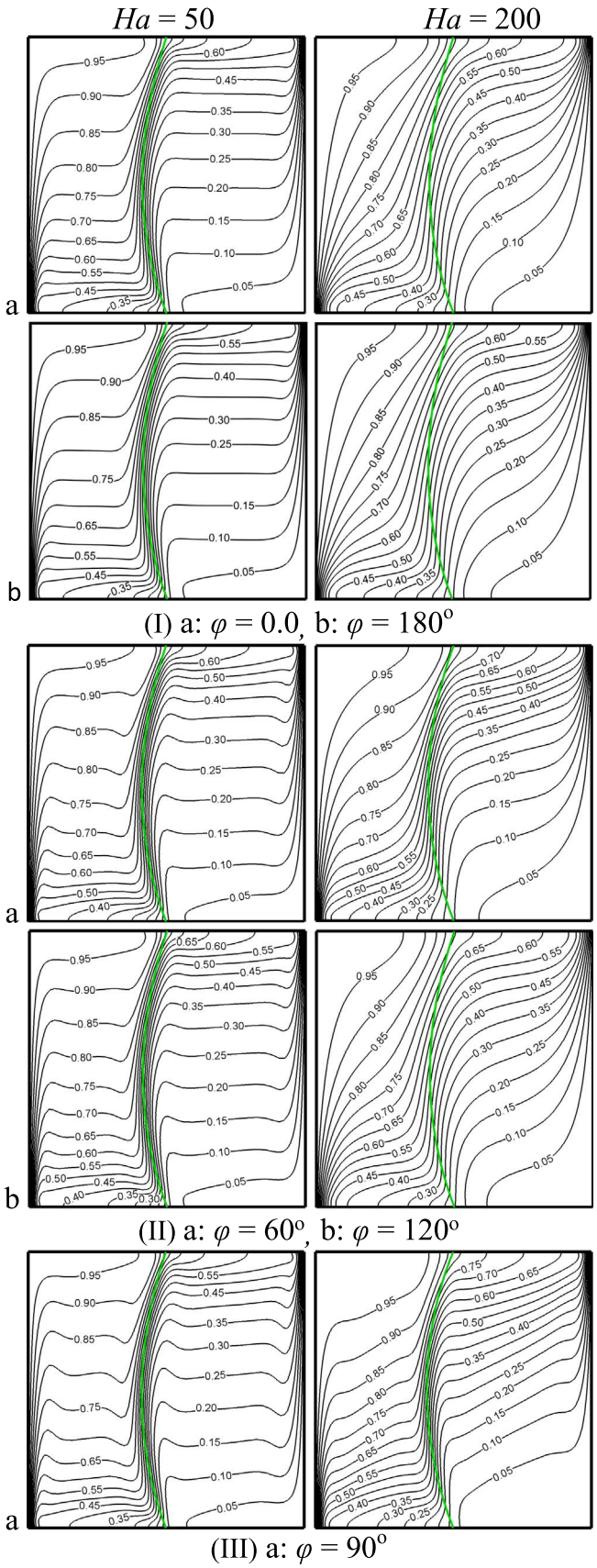

Fig. 13. Isotherms contours for Ha=50 and Ha=200 when Ra=10^7.

heat transfer gets stronger, the average Nusselt number also rises until it reaches its steady-state value. At the time scale around 10^{-2}, the average Nusselt number shows a significant increasing trend of behavior; this is where the heat transfer from the wall starts to affect the temperature distribution of the fluid in the hot cavity and changes

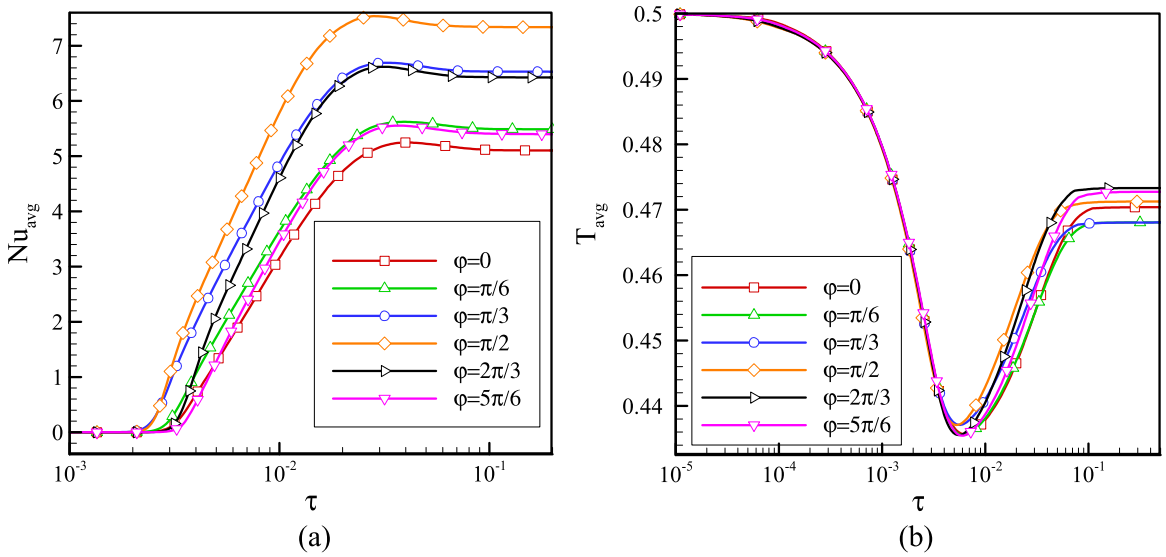

Fig. 14. The variations of average Nusselt number on the hot wall and dimensionless temprature versus the dimentionless time for the different values of φ at Ra=10^7, Ha=100.

the decay trend of the average temperature in the cavity into a rising trend.

Fig. 11 presents the influence of the Hartmann number on the steady state average Nusselt number and temprature for different values of Ra at φ=2π/3. It is observed that for a specified Hartmann number, the average Nusselt number and average fluid temprature increases and decreases with Ra, respectively. There is a downward trend of the Nusselt number as a function of the Hartmann number. However, a defined behavior does not exist for changes in the average temperature against Ha as is depicted in Fig. 11(b). As can bee seen, for an effective value of Ha (Ha≥50), the presence of the magnetic field enhances the dimensionless temperature at Ra=10^6–10^7, whereas the temperature decreases with Ha at Ra=10^8.

Fig. 12 presents the influence of φ on the steady state streamlines contours for various values of Ha at Ra=10^7. First, it is found that the strength of the fluid flow circulation increases as the magnetic field inclination angle increases until π/2 and then it begins to decrease with increasing φ beyond π/2 to π. This behavior refers to the diminishing of the magnetic force component acting in downward direction, which is opposite to the buoyancy forces. In addition, it can be seen that at the lower range of the Hartmann number (i.e. Ha=50), increasing the angle of the magnetic field inclination has no significant effects on the extension direction of the vortices formed, whereas for the higher Hartmann number (Ha=200), the streamlines are noticeably affected by the direction of the magnetic field. That is, the center of vortices inside the right and left sub-cavities shift up and down, respectively as the magnetic field inclination shifts away from the perpendicular fashion.

In case (II) of Figs. 12 and 13, the streamlines and isotherms counters for the two vertically symmetric angles of φ=π/3 and φ=2π/3 are compared. As seen, the streamlines and temperature distributions in the cases of φ=π/3 and φ=2π/3 are not the same. However, in case (I) where the results are compared for the inclination angles of φ=0 and φ=π, the results are perfectly the same. This result was predictable, because, as previously mentioned, the magnetic field term in the momentum equations is periodic with the period of π.

The influence of φ on the steady state isotherms contours for various values of Ha at Ra=10^7 are depicted in Fig. 13. The reduction of the fluid flow intensity because of the presence of the magnetic field and thus, reduction of the fluid thermal mixing, the isotherms tend to become mostly vertical. It is noticed also that the magnetic field inclination has no significant effects on the isotherms pattern, especially at the low values of Ha.

Fig. 14(a) and (b) illustrate that, at the initial steps of natural

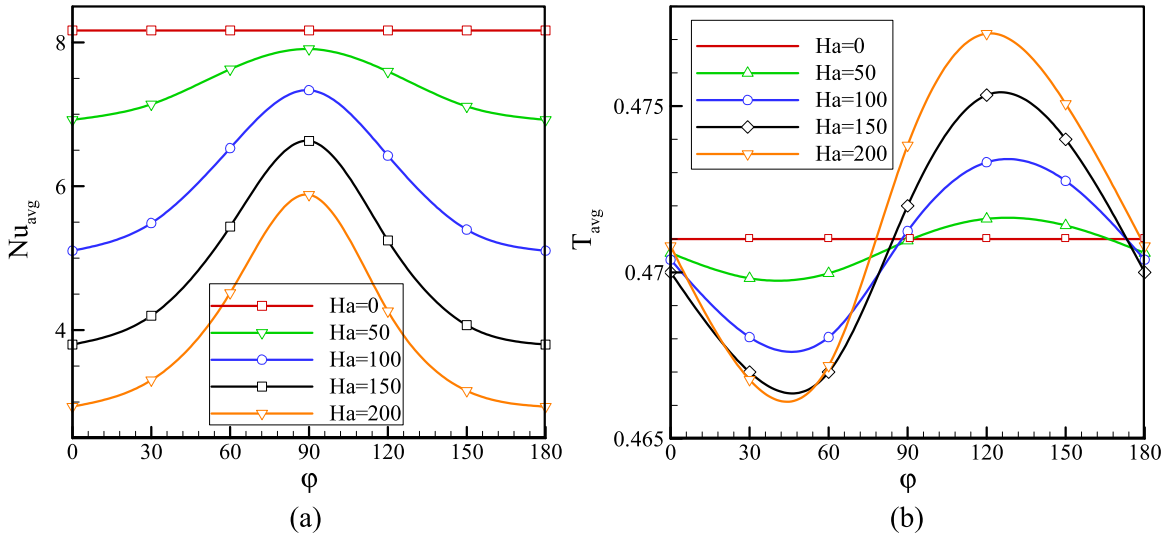

Fig. 15. Average Nusselt number on the hot wall and dimensionless temprature as function of inclination angle of magnetic field for the different values of Ha at Ra=10^7.

Table 1
The effect of Ra, Ha and φ on the maximum stresses σ_m induced in the flexible membrane.

Ra (Ha=50 and φ=2π/3)	σ_m	Ha (Ra=10^7 and φ=π/3)	σ_m	φ (Ra=10^7 and Ha=100)	σ_m
10^5	3.96853E+12	0	7.83326E+12	0	8.14466E+12
10^6	4.24432E+12	50	7.86271E+12	π/6	8.20718E+12
10^7	8.00369E+12	100	8.07708E+12	π/3	8.07708E+12
10^8	4.9871E+13	150	8.14157E+12	π/2	7.98819E+12
–	–	200	8.11824E+12	2π/3	8.11741E+12
–	–	–	–	5π/6	8.14691E+12

convection, the average Nusselt number and temperature are 0 and 0.5, respectively, for all values of φ. Then, the heat transfer rate grows due to the increase of fluid motion. It is interesting to note that the average temperature is the same for all the inclination angles of the magnetic field before reaching its minimum value. In addition, it is necessary to note that the reduction and then, augmentation of the average temperature until reaching its steady state condition is due to the exit and entry of the fluid as it has been explained previously.

Fig. 15(a) and (b) represent the variations of the average Nusselt number and the average fluid temperature at steady state according with inclination angle of magnetic field φ for different values of Ha. From Fig. 15(a), it is apparent that for a given value of Ha, except Ha=0, the average Nusselt number increases to reach its maximum at $\varphi=\pi/2$ and afterwards decreases to mostly reach the value recorded at φ=0. The peak values of the Nusselt number at $\varphi=\pi/2$ becomes steeper with increasing Ha. This means that orientating the magnetic field from the horizontal direction to the vertical direction can change its action from retardation of the buoyancy force to acceleration of the fluid originated from the heated wall. On the other hand, Fig. 15(b) shows that there is a quasi-sinusoidal trend for the temperature variation versus the inclination angle of the magnetic field. Here, it can also be seen that the amplitude of these quasi-sinusoidal curves grows with the rise of the magnetic field strength. Finally, we can say that the minimum and maximum values of the average temperature of the fluid occur at π/4 and 2π/3, respectively.

Fig. 15 which is in agreement with the streamline and isotherm contours depicted in Figs. 12 and 13 indicates that the values of T_{av} and Nu_{av} are identical for the two cases φ=0 and $\varphi=\pi$. However, the results are not symmetric about the vertical direction. This asymmetric behavior is also observed in Figs. 12 and 13.

The effects of the Rayleigh (Ra), Hartmann (Ha) and the angle of magnetic field orientation (φ) on the maximum stresses σ_m induced in the flexible membrane are illustrated in Table 1. When the Rayleigh number increases, the stress in the flexible number becomes more intense. This is due to the fact that increasing the Rayleigh number increases the strength of the fluid flow and accordingly, the interaction between the fluid and the flexible membrane augments. On the other hand, the results show that for Ra=10^7 and φ=π/3, an increase in Ha increases σ_m until Ha reaches 150. After that, as Ha increases from 150 to 200, a decrease in σ_m can be seen. Also, it is observed that although the increase of φ can change σ_m, but there is no certain trend for changing σ_m with φ. It can be observed that for Ra=10^7 and Ha=100, the maximum and minimum σ_m occurs at π/2 and π/6, respectively.

5. Conclusions

Unsteady natural convection inside a square cavity equally partitioned by a flexible impermeable membrane is investigated numerically using the finite element method with the arbitrary Lagrangian-Eulerian (ALE) technique. A uniform magnetic field is applied in different orientations to the cavity. The cavity is provided by two eyelets to compensate volume changes due the movement of the flexible membrane. The collected results have led to the following conclusions:

1. In the case of high values of the Hartmann numbers (Ha≥50), the presence of the magnetic field increases the dimensionless average temperature for moderate values of the Rayleigh number (Ra=10^6–10^7). However, in the case of high values of the Rayleigh number (Ra=10^8), the presence of a strong magnetic field decreases the dimensionless average temperature.
2. The fluid flow circulation is strengthened as the magnetic field inclination angle is increased from 0 up to π/2 and then it begins to decrease with further increase of φ to π.
3. For a given value of Ha (higher than zero), the average Nusselt number increases with the magnetic inclination angle to reach its maximum at $\varphi=\pi/2$ and afterwards decreases to mostly reach its value recorded at $\varphi=\pi$. The increment of the Nusselt number at $\varphi=\pi/2$ is steeper at higher value of the Hartmann number.
4. Depending on the angle of the magnetic field orientation and the Rayleigh number value, the increase of the magnetic filed could increase or decrease the induced stresses σ_m in the membrane.

In the present study, it is assumed that both of the sub-partitions are filled with only one type of fluid. However, in many practical applications, the membrane may be utilized to separate two different fluids. In this case, the electrical conductivity and other thermophysical properties of each sub-partition may be different. Considering a cavity filled with two different fluids could be the subject of future studies.

Acknowledgements

The first and second authors are grateful to Dezful Branch, Islamic Azad University, Dezful, Iran for its financial support.

References

[1] G.D. Davis, Natural convection of air in a square cavity: a bench mark numerical solution, Int. J. Numer. Methods Fluids 3 (1983) 249–263.
[2] T. Basak, S. Roy, I. Pop, Heat flow analysis for natural convection within trapezoidal enclosures based on heatline concept, Int. J. Heat. Mass Transf. 52 (2009) 2471–2483.
[3] R.S. Kaluri, R. Anandalakshmi, T. Basak, Bejan's heatline analysis of natural convection in right-angled triangular enclosures: effects of aspect ratio and thermal boundary conditions, Int. J. Therm. Sci. 49 (2010) 1576–1592.
[4] E.M. Alawadhi, Phase change process with free convection in a circular enclosure: numerical simulations, Comput. Fluids 33 (2004) 1335–1348.
[5] A. Al-Mudhaf, A.J. Chamkha, Natural convection of liquid metals in an inclined enclosure in the presence of a magnetic field, Int. J. Fluid Mech. Res. 31 (2004) 221–243.
[6] M. Sathiyamoorthy, A.J. Chamkha, Effect of magnetic field on natural convection flow in a square cavity for linearly heated side wall(s), Int. J. Therm. Sci. 49 (2010) 1856–1865.
[7] M. Sathiyamoorthy, A.J. Chamkha, Natural Convection flow under magnetic field in a square cavity for uniformly (or) linearly heated adjacent walls, Int. J. Numer. Method. H 22 (2012) 677–698.
[8] I.E. Sarris, S.C. Kakarantzas, A.P. Grecos, N.S. Vlachos, MHD natural convection in a laterally and volumetrically heated square cavity, Int. J. Heat. Mass Transf. 48 (2005) 3443–3453.
[9] N.S. Bondareva, M.A. Sheremet, I. Pop, Magnetic field effect on the unsteady natural convection in a right-angle trapezoidal cavity filled with a nanofluid: buongiorno's mathematical model, Int. J. Numer. Method. H 25 (2015) 1924–1946.
[10] A. Malvandi, M.R. Safaei, M.H. Kaffash, D.D. Ganji, MHD mixed convection in a vertical annulus filled with Al2O3–water nanofluid considering nanoparticle migration, J. Magn. Magn. Mater. 382 (2015) 296–306.
[11] A. Malvandi, Film boiling of magnetic nanofluids (MNFs) over a vertical plate in presence of a uniform variable-directional magnetic field, J. Magn. Magn. Mater. 406 (2016) 95–102.
[12] A. Malvandi, D.D. Ganji, Magnetic field effect on nanoparticles migration and heat transfer of water/alumina nanofluid in a channel, J. Magn. Magn. Mater. 362 (2014) 172–179.
[13] M.A. Sheremet, I. Pop, N.C. Rosca, Magnetic field effect on the unsteady natural convection in a wavy-walled cavity filled with a nanofluid: buongiorno's mathematical model, J. Taiwan Inst. Chem. Eng. 61 (2016) 211–222.
[14] A. Ben-Nakhi, A.J. Chamkha, Conjugate natural convection in a square enclosure with inclined thin fin of arbitrary length, Int. J. Therm. Sci. 46 (2007) 467–478.

[15] R. Jelti, S. Acharya, E. Zimmerman, Influence of baffle location on natural convection in partially divided enclosure, Numer, Heat. Transf. A 10 (1986) 521–536.
[16] N. Ben Cheikh, A.J. Chamkha, B. Ben Beya, Effect of inclination on heat transfer and fluid flow in a finned enclosure filled with a dielectric liquid, Numer, Heat. Transf. A 56 (2009) 286–300.
[17] S.H. Tasnim, M.R. Collins, Suppressing natural convection in a differentially heated square cavity with an arc shaped baffle, Int. Commun. Heat. Mass Transf. 32 (2005) 94–106.
[18] A.J. Chamkha, M. Mansour, S.E. Ahmed, Double diffusive natural convection in inclined finned triangular porous enclosures in the presence of heat generation/absorption effects, Heat. Mass Transf. 46 (2010) 757–768.
[19] C. Beckermann, S. Ramadhyani, R. Viskanta, Natural convection flow and heat transfer between a fluid layer and a porous layer inside a rectangular enclosure, ASME J. Heat. Transf. 109 (1987) 363–370.
[20] M.A. Sheremet, I. Pop, Conjugate natural convection in a square porous cavity filled by a nanofluid using Buongiorno's mathematical model, Int. J. Heat. Mass Transf. 79 (2014) 137–145.
[21] M. Mharzi, M. Daguenetb, S. Daoud, Thermosolutal natural convection in a vertically layered fluid-porous medium heated from the side, Energ. Convers. Manag. 41 (2000) 1065–1090.
[22] A.J. Chamkha, M.A. Ismael, Natural convection in differentially heated partially porous layered cavities filled with a nanofluid, Numer. Heat. Transf. A 65 (2014) 1089–1113.
[23] M.A. Ismael, A.J. Chamkha, Conjugate natural convection in a differentially heated composite enclosure filled with a nanofluid, J. Porous Media 18 (2015) 699–716.
[24] Y. Varol, H.F. Oztopa, I. Pop, Natural convection in a diagonally divided square cavity filled with a porous medium, Int. J. Therm. Sci. 48 (2009) 1405–1415.
[25] N. Tatsuo, Sh Mitsuhiro, K. Yuji, Natural convection heat transfer in enclosures with an off-center partition, Int. J. Heat. Mass Transf. 30 (1987) 1756–1758.
[26] N. Tatsuo, M. Shiraishi, F. Nagasawa, Y. Kawamura, Natural convection heat transfer in enclosures with multiple vertical partitions, Int. J. Heat. Mass Transf. 31 (1988) 1679–1686.
[27] H.F. Oztop, Y. Varol, A. Koca, Natural convection in a vertically divided square enclosure by a solid partition into air and water regions, Int. J. Heat. Mass Transf. 52 (2009) 5909–5921.
[28] K. Kahveci, Natural convection in a partitioned vertical enclosure heated with a uniform heat flux, ASME J. Heat. Transf. 129 (2007) 717–726.
[29] F. Xu, J.C. Patterson, Ch.W. Lei, Heat transfer through coupled thermal boundary layers induced by a suddenly generated temperature difference, Int. J. Heat. Mass Transf. 52 (2009) 4966–4975.
[30] E.V. Kalabin, M.V. Kanashina, P.T. Zubkov, Natural-convective heat transfer in a square cavity with time-varying side-wall temperature, Numer, Heat. Transf. A 47 (2005) 621–631.
[31] U. Küttler, W.A. Wall, Fixed-point fluid–structure interaction solvers with dynamic relaxation, Comput. Mech. 43 (2008) 61–72.
[32] M. Rahimi-Gorji, O. Pourmehran, M. Hatami, D.D. Ganji, Statistical optimization of microchannel heat sink (MCHS) geometry cooled by different nanofluids using RSM analysis, Eur. Phys. J. Plus 130 (2015) 1–21.
[33] M. Rahimi-Gorji, O. Pourmehran, M. Gorji-Bandpy, D.D. Ganji, An analytical investigation on unsteady motion of vertically falling spherical particles in non-Newtonian fluid by Collocation Method, Ain Shams Eng. J. 6 (2015) 531–540.
[34] W.S. Fu, W.J. Shieh, A study of thermal convection in an enclosure induced simultaneously by gravity and vibration, Int. J. Heat. Mass Transf. 35 (1992) (1965–1710).
[35] W.S. Fu, W.J. Shieh, Transient thermal convection in an enclosure induced simultaneously by gravity and vibration, Int. J. Heat. Mass Transf. 36 (1993) 437–452.
[36] H. Kimoto, H. Ishida, Vibration effects on the average heat transfer characteristics of the natural convection field in a square enclosure, Heat. Transf. Res 29 (2000) 545–558.
[37] W.S. Fu, W.W. Ke, K.N. Wang, Laminar forced convection in a channel with a moving block, Int. J. Heat. Mass Transf. 44 (2001) 2385–2394.
[38] L.A. Florio, A. Harnoy, Use of a vibrating plate to enhance natural convection cooling of a discrete heat source in a vertical channel, Appl. Therm. Eng. 27 (2007) 2276–2293 (Heat Powered Cycles-4).
[39] Y.P. Razi, K. Maliwan, M.C. Carrier-Mojitobi, A. Mojitobi, The influence of mechanical vibrations on buoyancy induced convection in porous media, in: K. Vafai (Ed.)Handbook of Porous Media, Taylor & Francis Group, LLC, 2005, pp. 321–370.
[40] S. Chung, K. Vafai, Vibration induced mixed convection in an open-ended obstructed cavity, Int. J. Heat. Mass Transf. 53 (2010) 2703–2714.
[41] L. Cheng, T. Luan, W. Du, M. Xu, Heat transfer enhancement by flow induced vibration in heat exchangers, Int. J. Heat. Mass Transf. 52 (2009) 1053–1057.
[42] M. Engel, M. Griebel, Flow simulation on moving boundary-fitted grids and application to fluid-structure interaction problems, Int. J. Numer. Method. Fluids 50 (2006) 437–468.
[43] M. Rahimi-Gorji, T.B. Gorji, Mofid Gorji-Bandpy, Details of regional particle deposition and airflow structures in a realistic model of human tracheobronchial airways: two-phase flow simulation, Comput. Biol. Med. 74 (2016) 1–17.
[44] M. Rahimi-Gorji, O. Pourmehran, M. Gorji-Bandpy, T.B. Ganji, CFD simulation of airflow behavior and particle transport and deposition in different breathing conditions through the realistic model of human airways, J. Mol. Liq. 209 (2015) 121–133.
[45] C.W. Hirt, A.A. Amsden, J.L. Cook, An arbitrary Lagrangian-Eulerian computing method for all flow speeds, J. Comput. Phys. 14 (14) (1974) 227–253.
[46] T.J.R. Hughes, W.K. Liu, T.K. Zimmermann, Lagrangian–Eulerian finite element formulation for incompressible viscous flows, Comput. Methods Appl. Mech. Eng. 29 (1981) 329–349.
[47] J. Donea, S. Giuliani, Jp Halleux, An arbitrary Lagrangian-Eulerian finite element method for transient dynamic fluid-structure interactions, Comput. Methods Appl. Mech. Eng. 33 (1982) 689–723.
[48] Fu Wu-Sh, Ch-P. Huang, Effects of a vibrational heat surface on natural convection in a vertical channel flow, Int. J. Heat. Mass Transf. 49 (2006) 1340–1349.
[49] S.K. Jena, V.K.R. Yettella, C.P.R. Sandeep, S.K. Mahapatra, A.J. Chamkha, Three dimensional Rayleigh–Bénard convection of molten gallium in a rotating cuboid under the influence of a vertical magnetic field, Int. J. Heat. Mass Transf. 78 (2014) 341–353.
[50] E. Jamesahar, M. Ghalambaz, A.J. Chamkha, Fluid–solid interaction in natural convection heat transfer in a square cavity with a perfectly thermal-conductive flexible diagonal partition, Int. J. Heat. Mass Transf. 100 (2016) 303–319.
[51] K. Khanafer, Comparison of flow and heat transfer characteristics in a lid-driven cavity between flexible and modified geometry of a heated bottom wall, Int. J. Heat. Mass Transf. 78 (2014) 1032–1041.
[52] J. Donea, A. Huerta, Finite Element Methods for Flow Problems, John Wiley, Sons, Chichester, 2003.
[53] S.W. Churchill, Free Convection in Layers and Enclosures, in: G.F. Hewitt (Ed.) Heat Exchanger Design Handbook, Section 2.5.8, Begell House, New York, 2002.